Journal of Structural Biology **127,** 64–71 (1999)
Article ID jsbi.1999.4141, available online at http://www.idealibrary.com on IDEAL®

Crystallization of the Human, Mitochondrial Voltage-Dependent Anion-Selective Channel in the Presence of Phospholipids

Max Dolder,*,[1] Kornelius Zeth,†,[2] Peter Tittmann,‡ Heinz Gross,‡ Wolfram Welte,† and Theo Wallimann*

*Institute of Cell Biology and ‡Institute of Applied Physics, Swiss Federal Institute of Technology, ETH-Hönggerberg, CH-8093 Zürich, Switzerland; and †Department of Biology, University of Konstanz, Universitätsstrasse 10, D-78434 Konstanz, Germany

Received December 17, 1998, and in revised form May 25, 1999

Overexpressed human voltage-dependent anion-selective channel VDAC or porin from mitochondrial outer membranes has been purified to homogeneity. Electron microscopic analysis of VDAC in detergent solution revealed a uniform particle population consisting of porin monomers. After dialysis of detergent-solubilized porin in the presence of dimyristoylphosphatidylcholine at lipid-to-protein ratios between 0.2 and 0.5 (percentage by weight), mostly multilamellar crystals were obtained. Crystals adsorbed to carbon films flattened during negative staining and air-drying and exhibited different structural features due to differences in the vertical stacking of several crystalline layers, each consisting of one membrane bilayer. Adsorbed, frozen-hydrated multilamellar membrane crystals revealed uniform diffraction patterns with sharp diffraction spots extending to 8.2 Å. The surface structure of VDAC was reconstructed from freeze-dried and unidirectionally metal-shadowed crystals. Major protein protrusions were observed from two VDAC monomers present in the unit cell. Differences in the surface structural features indicate alternate orientations of VDAC molecules with respect to the lipid bilayer, allowing the simultaneous imaging of both the cytosolic and intramitochondrial surfaces. Each VDAC molecule consists of a pore lumen with a diameter of 17–20 Å surrounded by a protein rim of nonuniform height, suggesting an asymmetrical distribution of protein mass around the diffusion channels.

Key Words: **electron microscopy; mitochondrial porin; membrane protein crystals; VDAC**

INTRODUCTION

The mitochondrial outer membrane is highly permeable to ions and hydrophilic solutes. This property is mediated by a 30- to 35-kDa pore-forming protein known as the voltage-dependent anion-selective channel (VDAC) or mitochondrial porin (for review see Benz, 1994; Colombini *et al.*, 1996; Thinnes and Reymann, 1997). At low transmembrane potential (<20 mV), these voltage-gated channels are slightly anion selective for equally mobile ions such as potassium and chloride (Ludwig *et al.*, 1989; Roos *et al.*, 1982). At higher transmembrane potential, porin channels switch to partially closed states, get less permeable for ions and charged metabolites, and exhibit cation selectivity (Benz *et al.*, 1990, 1988).

In addition to providing the major pathway for metabolites through the outer membrane, porin is also involved in contact site formation of the two mitochondrial envelopes (Brdiczka, 1991). When isolated from osmotically disrupted mitochondria, these contact sites are enriched in hexokinase as well as creatine kinase and nucleoside diphosphate kinase (Adams *et al.*, 1989). An important function of contact sites is believed to be in dynamic compartmentation of adenine nucleotides in the intermembrane space (Gellerich *et al.*, 1987) and high-energy phosphate channeling (Wallimann *et al.*, 1992). This concept is thought to prevent equilibration of the phosphorylation potential between the cytosol and the mitochondrial matrix (Brdiczka *et al.*, 1989).

Recently, it has been demonstrated that contact site complexes isolated from brain mitochondria, enriched in porin, adenine nucleotide translocator (ANT) of the inner mitochondrial membrane, and hexokinase or creatine kinase, when reconstituted in liposomes, exhibit certain characteristics of the mitochondrial permeability transition pore (PTP Beutner *et al.*, 1996; O'Gorman *et al.*, 1997). These findings suggest that porin, ANT, and hexokinase or creatine kinase probably also exist physiologically as complexes and may constitute a functional and struc-

[1] To whom correspondence should be addressed. Fax: ++41 1 633 10 69. E-mail: dolder@cell.biol.ethz.ch.

[2] Present address: Max-Planck-Institut für Biochemie, Abteilung Molekulare Strukturbiologie, Am Klopferspitz 18a, D-82152 Martinsried bei München, Germany.

1047-8477/99 $30.00

tural element of the PTP under conditions which favor its opening. Although the physiological function of PTP formation is still under debate (for review see Zoratti and Szabo, 1995), it has been hypothesized to be involved in cellular apoptosis (Petit *et al.*, 1996; Skulachev, 1996, 1998; Susin *et al.*, 1998) as well as in calcium signaling (Bernardi and Petronilli, 1996; Ichas *et al.*, 1997).

So far, the interactions among porin, ANT, and kinases in terms of compartmentation and complex formation have been described mainly on a functional level. Little is known about the structural elements involved in the direct physical interactions. Complex formation between porin and creatine kinase has been demonstrated to occur *in vitro* (Brdiczka *et al.*, 1994). The addition of porin to a N-terminal deletion mutant of creatine kinase, showing a marked reduction of octamer formation, was shown to induce octamerization of the latter, also indicating a direct interaction of the two proteins. From this observation, it was concluded that the domain of creatine kinase interacting with porin is different than the N-terminus (Brdiczka *et al.*, 1994). Furthermore, binding of hexokinase to porin may occur at sites near the C-terminal end of porin and the N-terminal end of hexokinase (Nakashima, 1989).

In view of our long-term goal of understanding these biologically significant interactions in more structural detail, we describe the preparation and electron microscopic characterization of membrane crystals of human type 1 porin (HVDAC1). Of the two human VDAC isoforms cloned and functionally expressed, HVDAC1 shows strong affinities to different kinases (Blachly-Dyson *et al.*, 1993). Protein crystals grew in the presence of phospholipids and exhibited three-dimensional stacking. The crystals described here represent the first successful attempt to crystallize a mammalian mitochondrial porin.

MATERIALS AND METHODS

Expression, Refolding, and Purification of HVDAC1

These steps were performed as described in detail in a forthcoming paper (Zeth *et al.*, manuscript submitted for publication). Briefly, HVDAC 1 was expressed at high levels in *Escherichia coli*. After harvesting and lysis of cells, inclusion bodies, containing all the expressed porin, were isolated and dissolved at a concentration of 10–15 mg of protein/ml in buffered 6 M guanidine hydrochloride. Refolding was achieved by dilution of solubilized proteins with 2% lauryldimethylamine oxide (LDAO) in refolding buffer (1 mM EDTA, 1 mM dithiothreitol, 20 mM Tris, pH 8). The solution was then concentrated and dialyzed against 0.1% LDAO in 50 mM sodium phosphate, pH 6. Final purification of properly folded protein and detergent exchange into 0.6% C_8E_4, 20 mM Tris, pH 8, was achieved by column chromatography using NiNTA medium and dialysis of the protein. The protein solution was stored at 4°C at a concentration of 6–10 mg/ml.

Preparation of Porin Crystals

The concentration of HVDAC1 was adjusted to 1 mg/ml with dialysis buffer containing 1% octyl-POE. Aliquots of the protein solution were mixed with an equal volume of DMPC (0.2–0.5 mg/ml in 1% octylpolyoxyethylene) to get a final lipid-to-protein ratio of 0.2–0.5. The mixtures were dialyzed at 25°C against 150 mM NaCl, 20 mM $MgCl_2$, 1 mM NaN_3, 10 mM MES, pH 6.5. Although the solutions became turbid after 4–5 h due to crystal formation, the dialysis time was extended to at least 48 h to completely remove the detergent. Samples were screened for crystal formation by conventional negative stain electron microscopy using 2% uranyl acetate.

Electron Microscopy

For vitrous ice embedding, a crystal suspension (5 µl) was applied to a glow-discharged, carbon-coated copper grid (400 mesh) for 1 min. After washing over two drops of distilled water, grids were blotted quickly and immediately frozen by plunging into liquid ethane. Grids were cryotransferred via a homemade high vacuum cryopreparation chamber (Midilab, Gross *et al.*, 1990) permanently attached to a Philipps CM12 cryo-TEM. Images were recorded at −175°C under low-dose conditions ($\leq$5 $e^-/Å^2$) at an acceleration voltage of 100 kV using a 1k slow-scan CCD camera (Gatan 694). The magnification was ×96 000, corresponding to a 2.5-Å pixel width on the specimen scale (pixel width of the CCD camera, 24 µm). Crystal quality and defocus (300–400 nm) were on line tested by FFT. For heavy metal shadowing, crystals were adsorbed to carbon-coated grids and washed as described above. Samples were then frozen in liquid nitrogen and transferred to the precooled cold stage of the Midilab. Freeze drying was carried out for 2 h at −80°C and under high vacuum conditions ($\leq 10^{-7}$ mbar). Samples were unidirectionally shadowed with tantalum/tungsten using an electron beam evaporator. The metal coat thickness (0.5 nm) was monitored with a Balzers QSG 301 quartz monitor. Single grids were then transferred on the precooled specially designed Gatan cryo-holder and images were recorded at ×77 000 magnification, corresponding to 3.1-Å pixel width on the specimen scale. At no stage were the specimens exposed to air or warmed up to ambient temperature. Under these conditions, a stabilizing carbon coat (C-baking), obscuring structural details, can be avoided. Correlation averaging and surface reconstructions were carried out using the in-house-developed Milan image processing package (Fuchs *et al.*, 1995). The resolution limits of the images were determined according to the spectral signal-to-noise ratio (Unser *et al.*, 1987). Since no symmetry was assumed for the unit cell, several images were necessary to obtain a complete surface reconstruction. Due to suppressed information perpendicular to the shadowing direction (Fig. 4b), a minimum of three images, each showing a view of the specimen shadowed from different directions, is required. Visualization of single particles by negative stain electron microscopy was achieved by deposition of a drop (5 µl) of detergent-solubilized porin (2–10 µg/ml) on a glow-discharged carbon-coated grid, washing with distilled water, and staining with 2% uranyl acetate.

RESULTS

Overproduction of C-terminally His-tagged HVDAC1 in *E. coli* and subsequent purification on NiNTA columns yielded highly purified porin with an apparent M_r of 35 kDa and essentially free of contaminating proteins (Fig. 1a). The protein was isolated from solubilised inclusion bodies and could be successively refolded (K. Zeth *et al.*, manuscript submitted for publication). Negative stain electron microscopy of purified VDAC dissolved in the non-

ionic detergent octyltetraoxyethylene (C_8E_4) revealed small particles with diameters of 35–40 Å (Fig. 1b). Single particles adsorbed randomly to glow-discharged carbon films. Some exhibited clear substructural features, with a stain-filled central region and a stain excluding outer portion (marked with arrows in Fig. 1b), indicating end-on views of porin molecules. The outer stain excluding part exhibited additional substructuration, particularly in the molecule indicated in the top right. Mass determination by quasi-elastic light scattering gave a value of 80 kDa for HVDAC1 in C_8E_4 (Zeth *et al.*, manuscript submitted for publication). This is consistent with the mass of one porin monomer binding the equivalent of one C_8E_4 micelle. From these observations we conclude that VDAC molecules are present as monomers in C_8E_4 solution. When reconstituted in the presence of dimyristoylphosphatidylcholine (DMPC), these monomers formed large crystalline structures as observed by negative stain electron microscopy (Fig. 2a). The lipid-to-protein ratio (LPR) exhibited an optimum for crystal formation between 0.2 and 0.5 (percentage by weight). Higher LPRs resulted in disordered, although dense, protein packing, whereas at LPRs below 0.2 the protein was found to be aggregated. Crystal sizes were heterogeneous, with the largest dimensions being up to 5 μm. At higher magnification, crystals turned out to be multilamellar (Fig. 2b). Occasionally, adsorbed crystals exhibited side views of the lamellae along the crystal border. Up to 10 layers, each with a thickness of 43 Å, can be distinguished in the example shown (white box in Figs. 2b and 2c), indicating that each layer represents one single lipid bilayer. No major protein protrusions on either side of the layers could be discerned in such views. The spacing between the layers showed some variations (Fig. 2b, arrowheads). Crystals with fewer layers than that shown in Fig. 2 were observed as well, but no single crystalline sheets. Crystals flattened on the carbon film during adsorption, staining, and air-drying. This resulted in the superposition of several crystalline layers and discrete steps in crystal thickness due to broken layers (Fig. 2b, white arrows) similar to those seen in thin 3D crystals of Ca^{2+}-ATPase (Stokes and Green, 1990). Although layers seemed to be in close contact over extended regions, the vertical stacking of the lamellae exhibited local variations. As a result, distinct structural patterns were observed when viewed in projection (see encircled areas in Fig. 2b). Differences in vertical stacking were easily discerned in negatively stained preparations but escaped detection in the low-contrast pictures of unstained, frozen-hydrated specimens. The best adsorbed, frozen-hydrated crystals diffracted to 8.2 Å (spot encircled in Fig. 3a). In the unstained averaged projection map (Fig. 3b), which represents the projection view through a crystal with several layers, dark regions correspond to high-density (protein), whereas bright regions represent low-density water-filled or lipid domains. The most prominent features are two low-density elliptically shaped areas per unit cell (unit cell dimensions: $a = 81.1 \pm 1.1$ Å, $b = 56.7 \pm 0.5$ Å, $\gamma = 110.4 \pm 0.6°$), surrounded by a high-density rim (indicated by the small arrows in Fig. 3b). Additional high-density areas are present at a distance from and with no obvious connection to the core structure (arrowheads in Fig. 3b). These features result from in-plane displacements of the individual superimposed crystalline layers, yielding a complex, not easily interpretable projection view.

As a consequence of the variations in three-dimensional stacking of these porin crystals, the collection of reliable volume data is not possible at

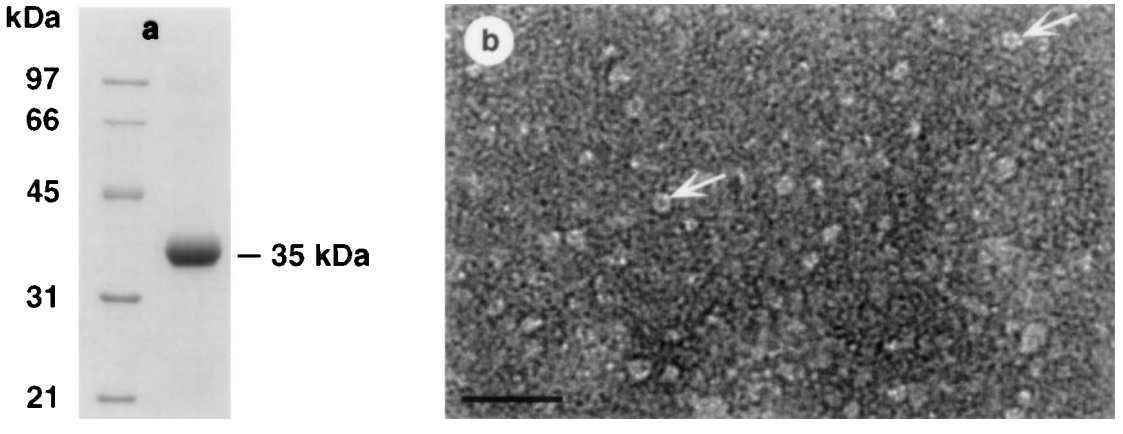

FIG. 1. (a) Sodium dodecyl sulfate–polyacrylamide gelelectrophoresis of HVDAC1 expressed in *Escherichia coli* and purified as described under Materials and Methods. Marker proteins (left) are indicated, with their molecular weights in kilodalton (kDa). (b) Negative stain electron micrograph of HVDAC1 dissolved in octyltetraoxyethylene (C_8E_4). White arrows point to particles revealing end-on views of monomeric VDAC molecules. Scale bar, 20 nm.

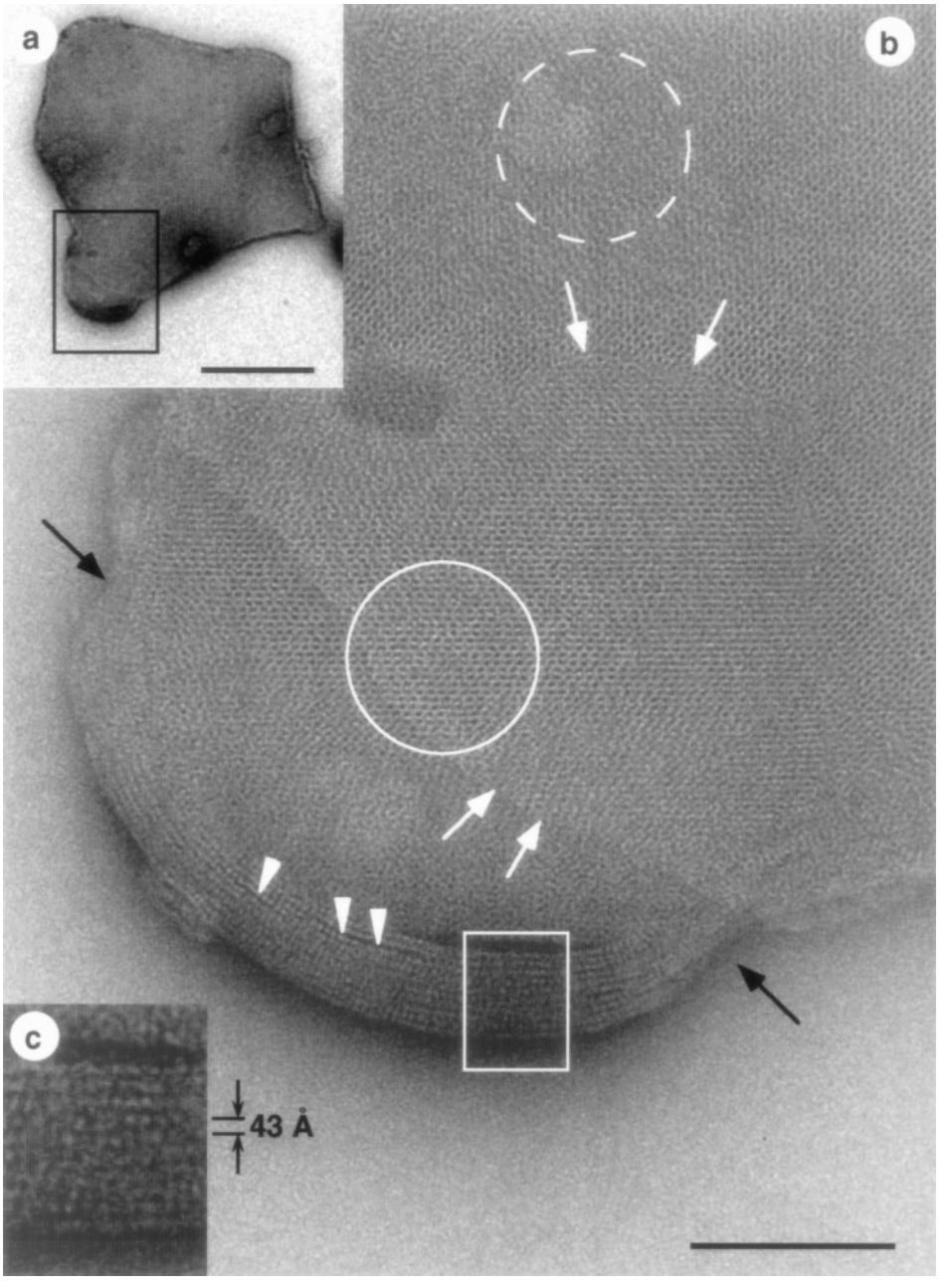

FIG. 2. (a) Negative stain electron micrograph of a multilamellar crystal observed after reconstitution of HVDAC1 in the presence of DMPC. (b) Higher magnification of the region outlined in (a). Steps in crystal thickness are indicated by white arrows. The multilamellarity is clearly visible along the crystal border between the two black arrows. White arrowheads show packing distortions of the lamellae. The region outlined by the full circle marks a crystal area with stacking of several layers in register, whereas in the region outlined by the dashed circle, stacking is out of register, resulting in a moiré pattern. The section enclosed by the white box is enlarged in (c). The measured thickness of 43 Å indicates that each layer represents one lipid bilayer. Scale bars are 500 nm in (a) and 100 nm in (b).

the moment. However, our main interest is concerned with the analysis of structural interactions of porin with peripherally bound kinases (see Introduction). These interactions are expected to be restricted to the surface-exposed protein domains. Therefore, we performed surface imaging by unidirectional and rotary shadowing of crystals to visualize the surface texture of VDAC. Figure 4a shows an overview of freeze-dried porin crystals unidirectionally shadowed with Ta/W. The periodic structure is barely visible at high magnification (Fig. 4b). The averaged structure (insert in Fig. 4b) clearly reveals the directional nature of the shadowing process (no information perpendicular to the shadowing direc-

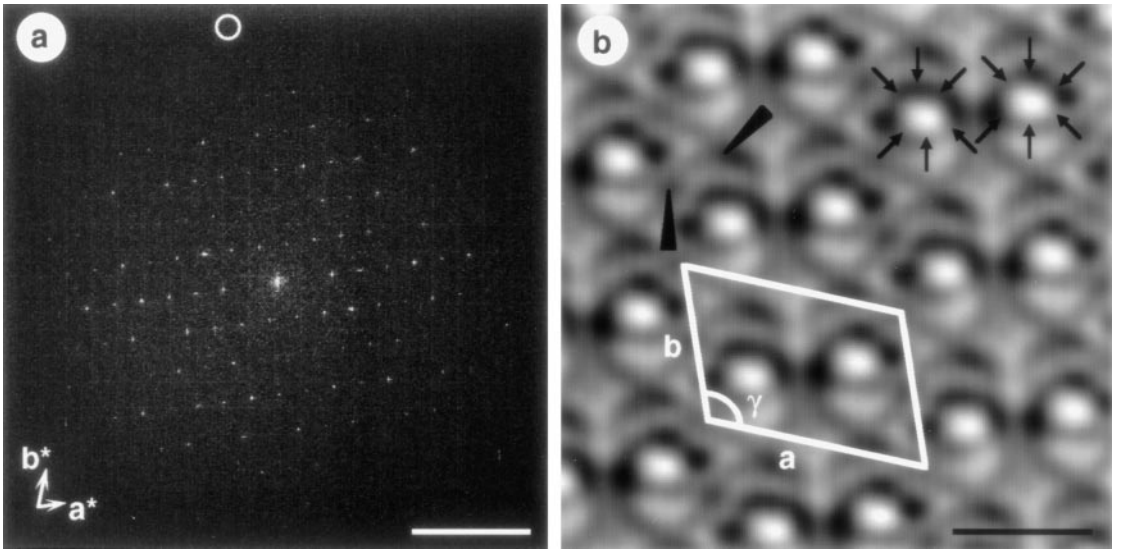

FIG. 3. Computed diffraction pattern (a) and corresponding correlation average (b) of a selected region of an adsorbed and vitrous ice-embedded HVDAC1 crystal. The diffraction pattern shows sharp spots extending to 8.2 Å (encircled). The reciprocal lattice vectors are indicated (a* and b*). The unit cell is outlined in the correlation average. Two low-density pore lumens surrounded by rims of higher density (marked with arrows in the top right) and additional contrast maxima (arrowheads) are the most prominent features in the unit cell. Scale bars represent 0.6 nm^{-1} in (a) and 5 nm in (b).

tion). Because this is true for the finest features resolved, decoration (preferential nucleation) and also the contrast of the underlying specimen itself can be neglected. The surface relief was reconstructed from six single images, each with a different shadowing azimuth. The main structural features are two deep holes per unit cell. Figure 4c shows a perspective view and Fig. 4d a top view (gray levels proportional to the height) of the reconstructed relief. The relief is compared with the averaged projection obtained from a rotary shadowed crystal (Fig. 4e). Although the lateral resolution of the averages of all single micrographs is very similar (15–16 Å), the correlation average from the rotary shadowing experiment displays finer structural details. This is due to the surface reconstruction process of an object without rotational symmetry. The calculation of the surface relief from several input images (at least three, here six) introduces a smoothing effect, with blurring of the finest structural features. However, protein domains protruding from the surface (indicated by asterisks in Figs. 4c–4e) as well as depressions between packed VDAC molecules (circles) are clearly resolved in the surface relief. The depressions represent the surface of the lipid bilayer between protein molecules. The unit cell (dashed parallelogram in Fig. 4e) houses two VDAC channels. The distribution of protein mass around the channel entrance is different in these two molecules. This is most clearly seen in Fig. 4e. In one molecule the central channel is oval shaped, whereas in the neighboring molecule the channel exhibits a triangular shape. The elevations seen between the two molecules represent protein masses contributed by the VDAC molecules. These elevations are not resolved such that they could be attributed to either one or the other channel molecule. From the differences in the structural features at the surfaces of the two VDAC molecules we conclude that they are inserted with opposite orientations into the lipid bilayer. Thus, one molecule exposes its cytosolic surface and the other one the surface facing the intermembrane space of mitochondria. The diameter of porin molecules, as measured from the surface relief, is 37 Å. This is in accordance with the measured size of single VDAC particles in solution (Fig. 1).

DISCUSSION

Here, we report on the successful crystallization of human mitochondrial porin (HVDAC1) and the electron microscopic characterization of membrane crystals grown in the presence of phospholipids. Starting from heterologously overexpressed, highly purified, monomeric porin, large multilamellar crystals were obtained under the conditions described in Materials and Methods. The reasons for multilamellar growth are not yet clear. Reduction of the concentration of divalent cations or their omission in the dialysis buffer resulted in disordered molecular packing but did not eliminate stacking of membrane layers. Similar effects were noted by variation of pH or partial replacement of DMPC by other lipids, including cholesterol. An important characteristic of the

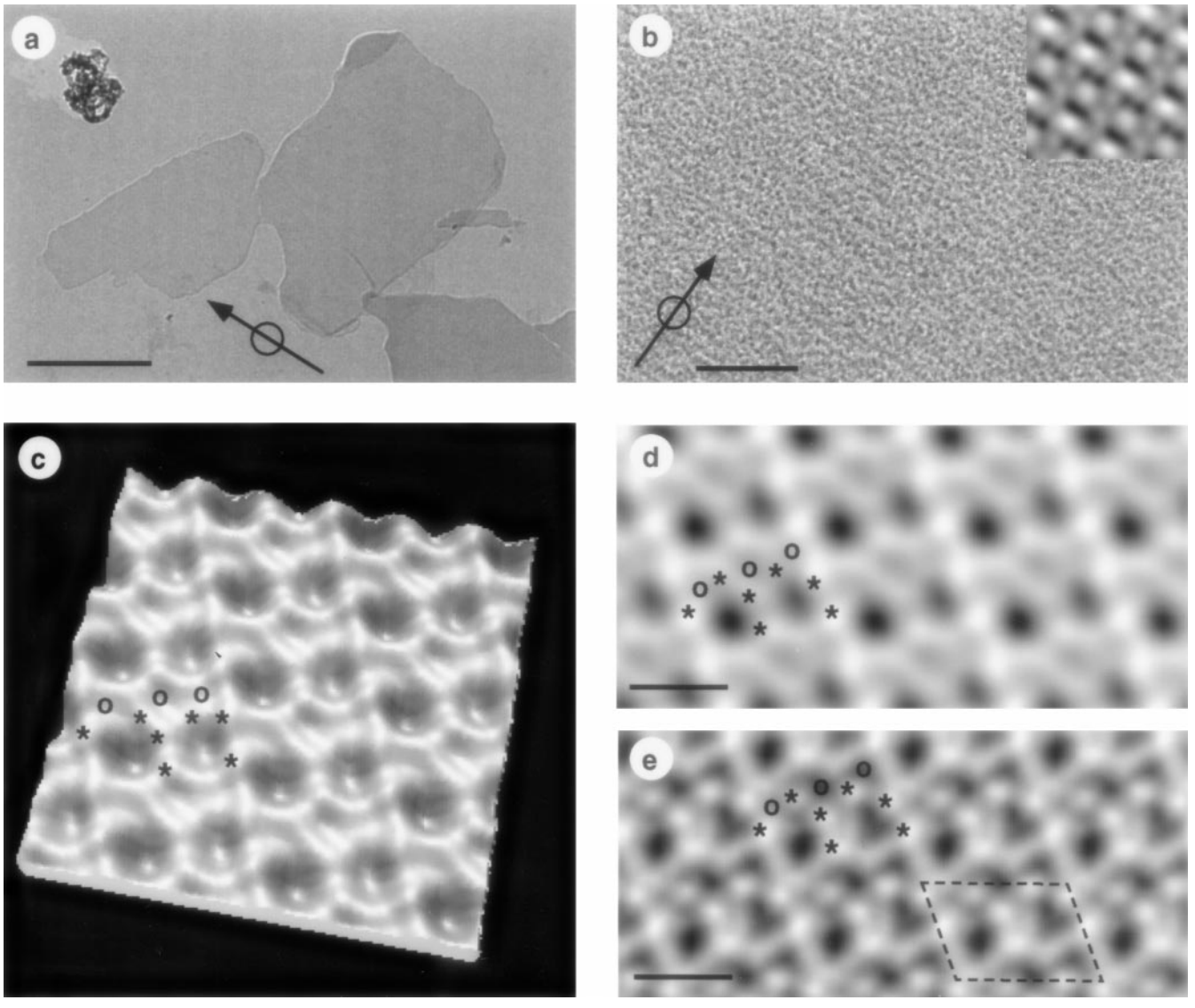

FIG. 4. (a) Low-magnification view of freeze-dried and unidirectionally shadowed VDAC crystals with Ta/W (elevation angle 45°). (b) High-magnification view of a crystalline region recorded from the large, flat crystal in (a) and corresponding correlation average (insert). The shadowing direction (indicated by the compasses in a and b) apparently changed due to a rotation of the image plane when switching from low to high magnification. Also shown are the three-dimensional perspective (c) and top view (d) of the reconstructed surface structure. The relief was calculated from six single images with different shadowing azimuths and an elevation angle of 65°. (e) Correlation average of a rotary-shadowed crystal (elevation angle 65°). The parallelogram-shaped unit cell is outlined. Asterisks in (c–e) mark the main protein protrusions and circles depressions between protein molecules (lipid bilayer level). Scale bars are 500 nm in (a), 20 nm in (b), and 5 nm in (d) and (e).

crystals presented here is that, due to common diffraction spots, it was not possible to separate the projections of individual layers by Fourier filtering. Therefore, correlation averages calculated from frozen-hydrated specimens gave superimposed projection views of several crystalline layers. Averaged projection maps of well ordered frozen-hydrated crystals revealed exclusively one lattice geometry with parallelogram-shaped unit cells and insignificant variations of lattice parameters (Fig. 3), suggesting strong lateral protein–protein and protein–lipid interactions. This is corroborated by our observation of large coherent crystalline patches in the *x–y* plane, indicating that crystals grew preferentially within this plane under the conditions used. The center-to-center distance measured from the surface relief of the two closest porin molecules is about 42 Å. Taking into account the 37-Å size of one molecule (measured at the surface), this leaves a space of 5 Å at most between each such pair of molecules. Thus, the lateral packing density in our crystals is comparable to that seen in two-dimensional VDAC crystals

obtained by phospholipase A_2 digestion of outer mitochondrial membranes of the fungus *Neurospora crassa* (Mannella, 1984; Mannella *et al.*, 1986). A major difference between the crystal structure presented in this study and that of *N. crassa* is the unit cell's content and the symmetry relationships. Whereas in *N. crassa* VDAC crystals six porin molecules are arranged in two groups of three channels related by twofold rotational symmetry (twofold axis perpendicular to the crystal plane, Guo and Mannella, 1993), we observed the presence of only two porin molecules per unit cell. The relief reconstruction as well as averages from freeze-dried rotary shadowed VDAC crystals showed that each pore lumen is surrounded by protein domains of variable height, and the in-plane rotational orientation of the two VDAC molecules per unit cell did not reveal a twofold symmetry. To explain these properties, we propose that the two porin monomers observed per unit cell are inserted with opposite orientation into the lipid bilayer. During biogenesis, porin is inserted into the outer mitochondrial membrane in a highly specific way and all porin molecules are likely to have the same orientation *in vivo* (Pfaller *et al.*, 1990). Therefore, alternate orientation of VDAC molecules in crystalline arrays is the result of the conditions used for reconstitution and is frequently observed in crystals of membrane proteins that were generated in the presence of phospholipids by starting from an isotropic solution (Kühlbrandt, 1992).

The nonuniform distribution of protein mass around the channel surface as seen in the relief is reminiscent to the stain excluding portions of negatively stained single VDAC particles (see Fig. 1b). For reasons discussed above, these substructures are barely recognized in averages of frozen-hydrated samples. The surface structure of VDAC as observed in our relief reconstruction clearly shows protein domains protruding from the bilayer surface. This is in agreement with a study to probe the transmembrane topology of VDAC in intact and broken bovine heart mitochondria using protease digestion (De Pinto *et al.*, 1991). As was shown in that report, several proteases have access to specific cleavage sites at both the cytosolic and the intramitochondrial surfaces of VDAC. In contrast, surface topographs obtained after freeze-drying and shadowing of crystalline arrays of *N. crassa* porin revealed that in these membranes, VDAC channels are deeply embedded in the bilayer without significant protein domains exposed at the surface (Thomas *et al.*, 1991). Therefore, differences in the surface topology of VDAC channels between different species seem to exist.

Mitochondrial porins are predicted to be composed of two-sided anti-parallel β-strands forming a β-barrel (De Pinto *et al.*, 1991; Mannella *et al.*, 1992) similar to that of bacterial porins, for which structural models at atomic resolution are available (Weiss *et al.*, 1991; Cowan *et al.*, 1992; Schirmer *et al.*, 1995; Forst *et al.*, 1998). The number of β-strands and their tilt angles relative to the membrane normal determine the pore diameter (Mannella, 1997). The diameter of the oval channel bore, measured from our surface reconstruction, is 17–20 Å. This is in agreement with the pore diameter estimated from single channel conductances (Benz, 1994). Together with the mean molecular diameter of HVDAC1 as measured here (37 Å), these values are compatible with 12–16 β-strands, with a certain proportion of strands tilted by more than 35° with respect to the membrane plane (Mannella, 1997).

The VDAC crystals reported here represent the first successful attempt to crystallize a mammalian porin. With these crystals, we are now in a position to study different aspects of the structural interaction of porin with soluble proteins of the cytosol and the mitochondrial intermembrane space. Our results represent a further step in the direction of identifying the structures of protein members involved in mitochondrial contact sites and the permeability transition pore.

We thank Dr. Volker Adams (Clinics for Cardiology, Heart Center Leipzig GmbH, Germany) for providing the expression plasmid for HVDAC1 and Professor Dieter Brdiczka (University of Konstanz) for comments on the manuscript. This work was supported by the Swiss National Science Foundation (Grant 31-50824.97 to T.W.), by the Stiftung für Wissenschaft und Forschung (SWF), and by private sponsoring (CAREAL Holding AG, Zürich).

REFERENCES

Adams, V., Bosch, W., Schlegel, J., Wallimann, T., and Brdiczka, D. (1989) Further characterization of contact sites from mitochondria of different tissues: Topology of peripheral kinases, *Biochim. Biophys. Acta* **981,** 213–225.

Benz, R. (1994) Permeation of hydrophilic solutes through mitochondrial outer membranes: Review on mitochondrial porins, *Biochim. Biophys. Acta* **1197,** 167–196.

Benz, R., Kottke, M., and Brdiczka, D. (1990) The cationically selective state of the mitochondrial outer membrane pore: A study with intact mitochondria and reconstituted mitochondrial porin, *Biochim. Biophys. Acta* **1022,** 311–318.

Benz, R., Wojtczak, L., Bosch, W., and Brdiczka, D. (1988) Inhibition of adenine nucleotide transport through the mitochondrial porin by a synthetic polyanion, *FEBS Lett.* **231,** 75–80.

Bernardi, P., and Petronilli, V. (1996) The permeability transition pore as a calcium release channel: A critical appraisal, *J. Bioenerg. Biomembr.* **28,** 129–135.

Beutner, G., Ruck, A., Riede, B., Welte, W., and Brdiczka, D. (1996) Complexes between kinases, mitochondrial porin and adenylate translocator in rat brain resemble the permeability transition pore, *FEBS Lett.* **396,** 189–195.

Blachly-Dyson, E., Zambronicz, E. B., Yu, W. H., Adams, V., McCabe, E. R., Adelman, J., Colombini, M., and Forte, M. (1993) Cloning and functional expression in yeast of two human

isoforms of the outer mitochondrial membrane channel, the voltage-dependent anion channel, *J. Biol. Chem.* **268,** 1835–1841.

Brdiczka, D. (1991) Contact sites between mitochondrial envelope membranes: Structure and function in energy- and protein-transfer, *Biochim. Biophys. Acta* **1071,** 291–312.

Brdiczka, D., Adams, V., Kottke, M., and Benz, R. (1989) Topology of peripheral kinases: Importance in transmission of mitochondrial energy, *in* Azzi, A., Nalecz, K. A., Nalecz, M. J., and Wojtczak, L. (Eds.), Anion Carriers of Mitochondrial Membranes, pp. 361–372, Springer-Verlag, Berlin.

Brdiczka, D., Kaldis, P., and Wallimann, T. (1994) In vitro complex formation between the octamer of mitochondrial creatine kinase and porin, *J. Biol. Chem.* **269,** 27640–27644.

Colombini, M., Blachly-Dyson, E., and Forte, M. (1996) VDAC, a channel in the outer mitochondrial membrane, *in* Narashi, T. (Ed.), Ion Channels, Vol. 4, pp. 169–202, Plenum, New York.

Cowan, S. W., Schirmer, T., Rummel, G., Steiert, M., Ghosh, R., Pauptit, R. A., Jansonius, J. N., and Rosenbusch, J. P. (1992) Crystal structures explain functional properties of two E. coli porins, *Nature* **358,** 727–733.

De Pinto, V., Prezioso, G., Thinnes, F., Link, T. A., and Palmieri, F. (1991) Peptide-specific antibodies and proteases as probes of the transmembrane topology of the bovine heart mitochondrial porin, *Biochemistry* **30,** 10191–10200.

Forst, D., Welte, W., Wacker, T., and Diederichs, K. (1998) Structure of the sucrose-specific porin ScrY from *Salmonella typhimurium* and its complex with sucrose, *Nature Struct. Biol.* **5,** 37–46.

Fuchs, K. H., Tittmann, P., Krusche, K., and Gross, H. (1995) Reconstruction and representation of surface data from two-dimensional crystalline, biological macromolecules, *Bioimaging* **3,** 12–24.

Gellerich, F. N., Schlame, M., Bohnensack, R., and Kunz, W. (1987) Dynamic compartmentation of adenine nucleotides in the mitochondrial intermembrane space of rat-heart mitochondria, *Biochim. Biophys. Acta* **890,** 117–126.

Gross, H., Krusche, K., and Tittmann, P. (1990) Recent progress in high-resolution shadowing for biological transmission electron microscopy, *in* Proceedings of the XIIth International Congress for Electron Microscopy, Seattle, pp. 510–511, San Francisco Press, San Francisco, CA.

Guo, X. W., and Mannella, C. A. (1993) Conformational change in the mitochondrial channel, VDAC, detected by electron cryomicroscopy, *Biophys. J.* **64,** 545–549.

Ichas, F., Jouaville, L. S., and Mazat, J.-P. (1997) Mitochondria are excitable organelles capable of generating and conveying electrical and calcium signals, *Cell* **89,** 1145–1153.

Kühlbrandt (1992) Two-dimensional crystallization of membrane proteins, *Q. Rev. Biophys.* **25,** 1–49.

Ludwig, O., Benz, R., and Schultz, J. E. (1989) Porin of Paramecium mitochondria isolation, characterization and ion selectivity of the closed state, *Biochim. Biophys. Acta* **978,** 319–327.

Mannella, C. A. (1984) Phospholipase-induced crystallization of channels in mitochondrial outer membranes, *Science* **224,** 165–166.

Mannella, C. A. (1997) On the structure and gating mechanism of the mitochondrial channel, VDAC, *J. Bioenerg. Biomembr.* **29,** 525–531.

Mannella, C. A., Forte, M., and Colombini, M. (1992) Toward the molecular structure of the mitochondrial channel, VDAC, *J. Bioenerg. Biomembr.* **24,** 7–19.

Mannella, C. A., Ribeiro, A., and Frank, J. (1986) Structure of the channels in the outer mitochondrial membrane, *Biophys. J.* **49,** 307–318.

Nakashima, R. A. (1989) Hexokinase-binding properties of the mitochondrial VDAC protein: Inhibition by DCCD and location of putative DCCD-binding sites, *J. Bioenerg. Biomembr.* **21,** 461–470.

O'Gorman, E., Beutner, G., Dolder, M., Koretsky, A. P., Brdiczka, D., and Wallimann, T. (1997) The role of creatine kinase in inhibition of mitochondrial permeability transition, *FEBS Lett.* **414,** 253–257.

Petit, P. X., Susin, S. A., Zamzami, N., Mignotte, B., and Kroemer, G. (1996) Mitochondria and programmed cell death: Back to the future, *FEBS Lett.* **396,** 7–13.

Pfaller, R., Kleene, R., and Neupert, W. (1990) Biogenesis of mitochondrial porin: the import pathway, *Experientia* **46,** 153–161.

Roos, N., Benz, R., and Brdiczka, D. (1982) Identification and characterization of the pore-forming protein in the outer membrane of rat liver mitochondria, *Biochim. Biophys. Acta* **686,** 204–214.

Schirmer, T., Keller, T. A., Wang, Y.-F., and Rosenbusch, J. P. (1995) Structural basis for sugar translocation through maltoporin channels at 3.1 Å resolution, *Science* **267,** 512–514.

Skulachev, V. P. (1996) Why are mitochondria involved in apoptosis? Permeability transition pores and apoptosis as selective mechanisms to eliminate superoxide-producing mitochondria and cell, *FEBS Lett.* **397,** 7–10.

Skulachev, V. P. (1998) Cytochrome c in the apoptotic and antioxidant cascades, *FEBS Lett.* **423,** 275–280.

Stokes, D. L., and Green, N. M. (1990) Three-dimensional crystals of CaATPase from sarcoplasmic reticulum, *Biophys. J.* **57,** 1–14.

Susin, S. A., Zamzami, N., and Kroemer, G. (1998) Mitochondria as regulators of apoptosis: Doubt no more, *Biochim. Biophys. Acta* **1366,** 151–165.

Thinnes, F. P., and Reymann, S. (1997) New findings concerning vertebrate porin, *Naturwissenschaften* **84,** 480–498.

Thomas, L., Kocsis, E., Colombini, M., Erbe, E., Trus, B. L., and Steven, A. C. (1991) Surface topography and molecular stichiometry of the mitochondrial channel, VDAC, in crystalline arrays, *J. Struct. Biol.* **106,** 161–171.

Unser, M., Trus, B. L., and Steven, A. C. (1987) A new resolution criterion based on the spectral signal to noise ratio, *Ultramicroscopy* **23,** 39–51.

Wallimann, T., Wyss, D., Brdiczka, D., Nicolay, K., and Eppenberger, H. M. (1992) Intracellular compartmentation, structure and function of creatine kinase isoenzymes in tissues with high and fluctuating energy demands: The PCr-circuit for cellular energy homeostasis, *Biochem. J.* **281,** 21–40.

Weiss, M. S., Abele, U., Weckesser, J., Welte, W., Schiltz, E., and Schulz, G. E. (1991) Molecular architecture and electrostatic properties of a bacterial porin, *Science* **254,** 1627–1630.

Zoratti, M., and Szabo, I. (1995) The mitochondrial permeability transition, *Biochim. Biophys. Acta* **1241,** 139–176.